Journal of Materials Chemistry A

ZnS Quantum Dots@MultilayeredCarbon: Geological-Plate-Movement-Inspired Designfor High-Energy Li-ion Batteries

Journal:	*Journal of Materials Chemistry A*
Manuscript ID	TA-ART-02-2018-001667.R1
Article Type:	Paper
Date Submitted by the Author:	21-Mar-2018
Complete List of Authors:	Fang, Daliang; Institute of Process Engineering Chinese Academy of Sciences; University of the Chinese Academy of Sciences Chen, Shimou; Institute of Process Engineering, Chinese Academy of Sciences, Wang, Xi; Beijing Jiaotong University; Tianjin University Tianjin 300072, P. R. China Bando, Yoshio; National Inst for Materials Science, Advanced Materials Lab and Nanomat Lab Golberg, Dmitri; National Institute for Materials Science; Queensland University of Technology Zhang, Suojiang; Institute of Process Engineering, Chinese Academy of Sciences,

Journal Name

ARTICLE

ZnS Quantum Dots@MultilayeredCarbon: Geological-Plate-Movement-Inspired Designfor High-Energy Li-ion Batteries

Received 00th January 20xx,
Accepted 00th January 20xx

DOI: 10.1039/x0xx00000x

www.rsc.org/

Daliang Fang,[ab] Shimou Chen,*[a] Xi Wang,*[cd] Yoshio Bando,[e] Dmitri Golberg,[ef] and Suojiang Zhang*[a]

Nowadays, much process has been made in designing practical high-energy-density anode materials for lithium-ion batteries (LIBs). However, during repeated charge-discharge cycles, high-energy-density anode materials usually undergo large volume changes, which cause limited cycle life. The situation would be worse, when anode materials have high tap densities and low porosities. Here, inspired by that Earth can release its inner stresses to maintain its structure stability through geological plate movements, a novel slippage-strategy is proposed to tackle the above problem. We fabricate a ZnS quantum dots@multilayered N-doped carbon matrix (ZnS-QDs@mNC), where ZnS quantum dots are well dispersed in N-doped carbon nanosheets, which assemble into micro-sized particles by intertwined overlapping. *In-situ* transmission electron microscopy demonstrates that carbon nanosheets of ZnS-QDs@mNC could slide against each other during lithiation just as geological plate movements, which canhelpmake full use of the limited gaps between carbon nanosheets to reduce the volume expansion of ZnS-QDs@mNC anode to only 6.5% (far below the industrial acceptable value of ~30%). As a result of the structural stability, ZnS-QDs@mNC with a high tap density of 0.86 g cm^{-3} and a low total pore volume of 0.092 cm^3 g^{-1} demonstrates excellent Li-storage properties even when the areal capacity is increased to 1.82 mAh cm^{-2}.

Introduction

There is a high demand to fabricate advanced anode materials with high energy densities to meet the requirements of rapidly developing electric vehicles' market and smart electrical grids.[1-3]Graphite, as a commercial anode material, has reached its limited theoretical capacity of 372 mAh g^{-1}.[4] Although silicon, metal oxides and metal sulfides have 2~11 times higher theoretical capacities than graphite,[5-8]the application of them as LIBs anodes has seriously been hindered because of huge volume changes (100~300%) during cycling. The stresses caused by volume changes lead to pulverization of anode materials, which results in poor cycling stability.Nanostructuring using carbon coating has been proved to be an effective way to solve the problem.[5-8]Up to now, various nanostructures of silicon, metal oxides and metal sulfides have been investigated as LIBs anodes and most of them, indeed, exhibit significantly enhanced Li-storage performances.[9-11] However, only a few of these large-volume-change anode materials have been commercialized taken into account the required low tap density (<< 1.0 g cm^{-3}) and severe side reactions after nanostructuring.

In order to achieve practical use of large-volume-change anode materials, the main strategy is to embed nano-size active materials into micro-size carbon frameworks with hierarchically ordered structures. For example, Cui et al.[12]designed a pomegranate-inspired silicon-based anodes, in which silicon nanoparticles are well dispersed in micro-sized carbon matrix with a hierarchically structure resembling a natural pomegranate. The composites possess high volumetric capacity of 1270 mAh/cm^3 and long cycling stability. Yu et al.[13] developed a general way to synthesize metal sulfides (NiS, CoS and MnS) nanoparticles embedded in a micro-size interconnected carbon matrix, which exhibits excellent lithium ions storage performances and high volumetric capacities. Recently, inspired by a watermelon shape, Guoet al.[14] developed a Si/C microspheres, which presents outstanding cycling stability and rate performance even at a high areal capacity. Indeed, these works have documented a great progress in achieving the practical goals of large-volume-change anode materials design. However, in order to realize long cyling stability, these works need to fabricate many voids or gaps in their anode materials to accommodatevolume changes of active materials upon the repeated lithiation/dislithiation. Nevertheless, these voids or gaps would reduce the tap densities of these anode materials significantly. Therefore, it is a big challenge to effectively accommodate large volume changes of anode materials with low porosities and high tap densities, and more novel strategies are still needed.[15]

[a]*Beijing Key Laboratory of Ionic Liquid Clean Process, Key Laboratory of Green Process and Engineering, Institute of Process Engineering, Chinese Academy of Sciences, Beijing 100190, P. R. China*
[b]*University of Chinese Academy of Sciences, Beijing 100049, China*
[c]*Key Laboratory of Luminescence and Optical Information, Ministry of Education, School of Science, Beijing Jiaotong University, Beijing, 100044, P. R. China*
[d]*Tianjin Key Laboratory of Molecular Optoelectronic Sciences, Department of Chemistry Tianjin University, and Collaborative Innovation Center of Chemical Science and Engineering (Tianjin), Tianjin 300072, P. R. China*
[e]*World Premier International Center for Materials Nanoarchitectonics (WPI-MANA) National Institute for Materials Science (NIMS), Namiki 1-1, Tsukuba 305-0044, Japan*
[f]*Queensland University of Technology (QUT), 2 George St., Brisbane, QLD 4000, Australia*
Electronic Supplementary Information (ESI) available: [details of any supplementary information available should be included here]. See DOI: 10.1039/x0xx00000x

ZnS is an attractive anode material for LIBs due to its high theoretical capacity of 900 mAh/g and natural abundance.[16]However, ZnS also suffers from the large volume change (~ 110%). Therefore, in this work, we choose ZnS as an example of a large-volume-change anode material. Inspired by that Earth can release its inner huge stresses to maintain its structure stability through geological plate movements, we design a ZnS quantum dots@multilayered N-doped carbon matrix composite (ZnS-QDs@mNC) with hierarchically ordered structure formed by an intertwined overlap of ZnS quantum dots@carbon nanosheets (ZnS-QDs@CNSs) building blocks. The *in-situ*transmission electron microscopy (TEM) demonstrates that, when lithiated, carbon nanosheets can slide against each other，similar to the plate movement on Earth.The slippage behaviour can effectively accommodate large volume changes of ZnS-QDs by making full use of the limited gaps between carbon nanosheets. As a result, the volume expansion of the ZnS anode is only 6.5%, far below the industrial requirement of 30%, even with a high tap density of 0.86 g cm^{-3} and a low total pore volume of 0.092 cm^3 g^{-1}. Due to excellent structure stability, ZnS-QDs@mNC exhibits a high reversible capacity of 887mAh g^{-1} and retains 77% of its initial capacity after 300 cycles at a high current density of 840 mA/g. Stable cycling can still be obtained even at a high areal capacity of 1.82 mAh cm^{-2}. This work provides a new avenue for designing practical high-energy-density anode materials for LIBs.

Result and discussion

The synthesis process of ZnS-QDs@mNC is shown in Figure 1a. In this work, ZIF-7 was synthesized using a typical solvothermal method. Figure S1 depicts the powder X-ray diffraction patterns of the products, which match well with previous results published,[17] confirming the products as ZIF-7 with good crystallinity. The TEM image in Figure S2a indicates that the produced ZIF-7 is mainly composed of thin hexagonal nanosheets (NSs) with a size ranging from 30 to 50 nm. After solution evaporation, these ZIF-7 NSs tend to aggregate together to form ZIF-7 micro-particles (MPs) with size ranging from 4 to 30 μm, as shown in Figure S2b. The magnified SEM image illustrates that ZIF-7 MPis a multi-layered structure (Figure S2c), as a result of a large number of ZIF-7 NSs stacked together (Figure S2d). After mixing with some sulfur powders, ZIF-7 MPs used as precursors were sealed in a glass vacuum tube and then heated at 600℃ for 1h. During the heating process, the sulfur powders sublimated into gas and reacted with Zn of ZIF-7 to formZnS-QDs. And at the same time, the carbonization of organic ligands within ZIF-7 NS into CNSwas accelerated by sulfur vapor,[18] hence, in situ generated ZnS-QDs were immediately encapsulated by CNS to form ZnS-QDs@CNS. Then those ZnS-QDs@CNS would stick together tightly to form ZnS-QDs@mNC under the high pressure caused by sulfur vapors. After cooling and taking out of the vacuum tube, the ZnS-QDs@mNC composites were ball milled into micro-particles with a size ranging from 0.5-13.5 um and an average size of around 5.5 um (Figure 1b). Such wide size distribution was beneficial for making materials with high tap density. As a result ,the as-synthesized ZnS-QDs@mNC exhibited a high tap density of 0.86 g cm^{-3}, which is close to that of commercial graphites (1.0 g cm^{-3}), see Figure 1c. The powder X-ray diffraction of ZnS-QDs@mNC shows that the three diffraction peaks appearing at 28.6°，47.6°and 56.6°correspond to (111), (220) and (311) planes of the zinc blende phase of ZnS (Figure 2a).[19] The low peak intensities and broad peaks demonstrate the nanosized feature of ZnS particles.[20] Meanwhile,no diffraction peaks fromprecursors or impurities were observed, demonstrating a completeconversion of ZIF-7 MP into ZnS-QDs@mNC during the sulfurization process. Raman spectra analysis was carried to study the carbon matrices of ZnS-QDs@mNC, as shown in Figure 2b. The two broad peaks located at 1335 and 1595 cm^{-1} can be respectively assigned to typical D- and G-bands of carbon.[20] The ID/IG ratio is 1.07, demonstrating that the carbon in the composite is indeed partially graphitic. The nitrogen species of ZnS-QDs@mNC were investigated by High-resolutionX-ray photoelectron spectrometer (XPS). As shown in Figure 2c, the spectra exhibits three peaks, which correspond to the pyridinic (398.6 eV), pyrrolic (400.2 eV), and graphitic (401.4 eV)nitrogen forms,[20] respectively. This evidence confirms that the nitrogen was successfully doped into the resultant porous carbon structure during the carbonization of N-containing organic ligands of ZIF-7. Such nitrogen doping can not only significantly improve electronic conductivity of carbonaceous materials, but also enhance Li-ion storage properties by introducing more hole defects, which is also beneficial for buffering volume change.[21] The nitrogen adsorption measurements of ZnS-QDs@mNC shows a Brunauer–Emmett–Teller surface area of 31.74 m^2 $g^{-1}$with a total porevolume of 0.092 cm^3g^{-1} (Figure 2d). The low surface area can reduce the contact between electrolyte and anode materials, thus avoiding severe side reactions. The pore-size distribution plot reveals a pore size in the range of 1-5 nm, implying two types of pores, i.e. micropores and mesopores, in the ZnS-QDs@mNC composite. The pores can facilitate the penetration of electrolyte and accommodate the volume changes of ZnS quantum dots during cycles

In order to investigate the structure of composites, scanning electron microscopy (SEM) and transmission electron microscopy (TEM) were applied, seeFigure 1d-g. Figure 1d shows thatZnS-QDs@mNC is multi-layered and composed of a large number of thin carbon nanosheets stacked together, which is consistent with the TEM image of ZnS-QDs@mNC shown in Figure 1e. The inset image of Figure 1e presents the schematic illustration of the intertwined overlap of those carbon nanosheets, which creates many gaps between those nanosheets, being beneficial for reducing volume expansion. Figure 1e reveals that a large number of ZnS nanoparticles with a size around a few nanometers (black dots) are well distributed in those thin carbon sheets (grey matrix). The magnified TEM image demonstrates that the grain size of ZnS nanoparticles is around 5 nm (Figure 1f), which is small enough to shorten pathways of lithium ions and electrons. As shown in Figure 1g, the lattice fringes with a spacing of 0.31 nm correspond to (111) interplane distance of ZnS.[22] The EDS mapping of ZnS-QDs@mNC confirms the co-existence and the homogenous distribution of Zn, S, N elements within the multi-layered carbon framework (Figure S3a-e). The mass percentage of ZnS in the ZnS-QDs@mNCcomposites was quantified by thermogravimetric analysis (TGA) at a heating rate of 5 ℃/min in dry air(Figure S4). The mass loss of about 4% below 250 ℃ could be ascribed to the loss of absorbed water. The

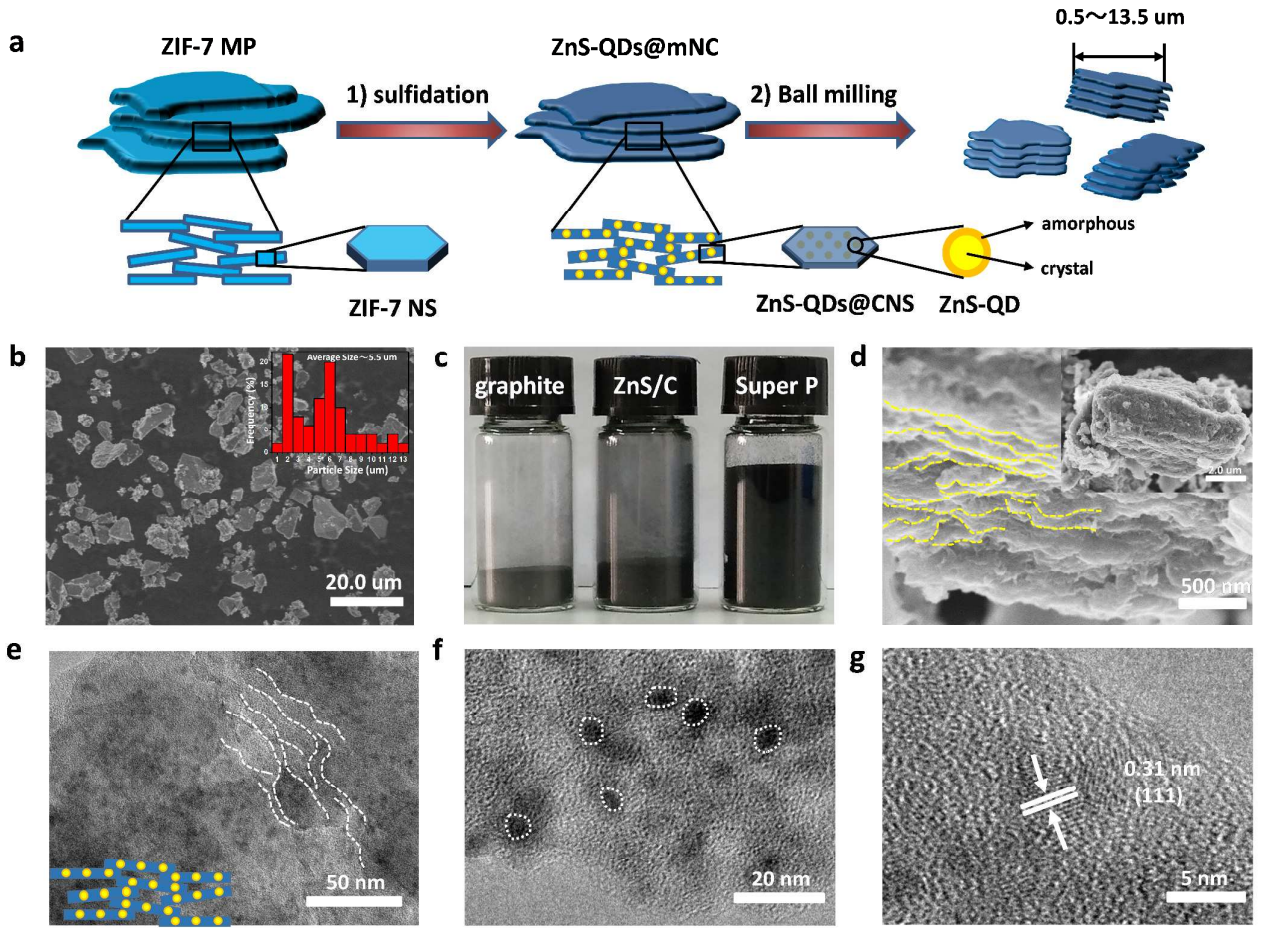

Figure 1. a) Schematic illustration for the formation of ZnS-QDs@mNC composites. b) SEM image of ZnS-QDs@mNC after milling. The inset is the statistical analysis of the distribution of the size of ZnS-QDs@mNC based on (b). c) Volume comparison on tightly packed samples. From left to right, 0.4 g commercial graphites, 0.4 g ZnS-QDs@mNC composites, and 0.4 g commercial Super P, respectively. d) Magnified SEM image of the side face of one ZnS-QDs@mNCpaticle.The edges of carbon nanosheets are marked by yellow dashed lines. Inset image shows the top face of the ZnS-QDs@mNC. e) Low magnification TEM of ZnS-QDs@mNC. The boundary lines of carbon nanosheets were marked by white dashed lines. f) Magnified TEM and g) HR-TEM images of ZnS-QDs@mNC.

weight loss of about 34% from 350 to 520 ℃can correspond to the combustion of carbon.[23] And the last weight loss on the TGA curve, which is seen between 520 and 640 ℃, is due to the oxidation process of ZnS.[17] Therefore the ZnS content is calculated as(46.27%*119%)/ 95.97%=57.37%, according to the weight change of 119% from ZnO to ZnS.[24]

To test the practical application of the as-designed structure, ZnS-QDs@mNC was evaluated as anode materials for lithium-ion batteries. In order to avoid overestimation, all the specific capacities in this work were calculated according to the total mass of the composites. Figure S5a shows the charge-discharge voltage profiles of ZnS-QDs@mNC for the first cycle at a current density of 140mA g^{-1} within the potential range of 0.01-3.0V vs. Li/Li^+. The discharge potential plateau that appears in 0.6-0.9 V corresponds to a lithiation process, while the charge potential plateau in 1.2-1.5 V to the dislithiation process. The discharge and charge capacities in the first cycle are 1243 and 887 mAh g^{-1}, respectively, corresponding to the initial Coulombic efficiency of 71%. Figure S5b shows the first four cycles of the cyclic voltammetry (CV) for ZnS-QDs@mNC tested at a san rate of 0.1 mV s^{-1} in the potential range of 0.01-2.5 V. The broad peak in the potential range of 0.9-0.05 V observed in the first cathodic sweep is attributed to the lithiation of ZnS into metallic Zn and Li_2S , the alloying process of Zn-Li and the formation of a solid electrolyte interphase (SEI) from the decomposition of electrolyte, which is consistent with the discharge potential plateau in Figure S5a. In the anodic sweeps, the oxidation peak at 1.3 V could be related to the regeneration of ZnS,[25] which is also proved by the charge potential plateau in Figure S5a. Except the first cycle, the other curves almost overlap, indicating good reversibility and stability.[26]

The cycling stability is further demonstrated by the galvanostatic method in Figure 3a. At a high current density of 840 mA g^{-1}, after 300 cycles, ZnS-QDs@mNC maintains a reversible capacity of 506 mAh g^{-1} with approximately 77% capacity retention, responding to a

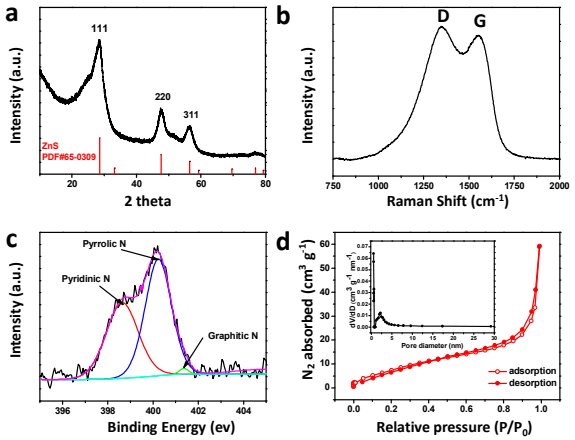

Figure 2.a) XRD patterns; b) Raman spectra;c) High-resolution N 1s XPS spectra; d) N2 sorption isotherms of ZnS-QDs@mNC (inset shows the pore-size distribution calculated using the BJH method).

low capacity fading of only 0.07%per cycle. In addition, except the first two cycles, the Coulombicefficiency maintains above 98.3% in the subsequentcycles. By contrast, only after 50 cycles, the reversible capacity of pure ZnS becomes only 123 mAh g^{-1}. Figure 3b reveals the rate performance of ZnS-QDs@mNC at various current densities from 140 to 4200 mA g^{-1}. The capacity decreases moderately along with the increase of current density. Even at the high current density of 4200 mA g^{-1}, the capacity of ZnS-QDs@mNC can still reach over 500 mAh g^{-1}. Note that, after the current density is changed back to 140 mA g^{-1}, the capacity of ZnS-QDs@mNC reverts to the original values, demonstrating the good reversibility of the electrode material. The excellent rate performances could be ascribed to ZnS-QDs well dispersed in the carbon matrix, which benefits fast transport of electrons and penetration of Li ions. It is known that achievement of high areal mass loading is of key

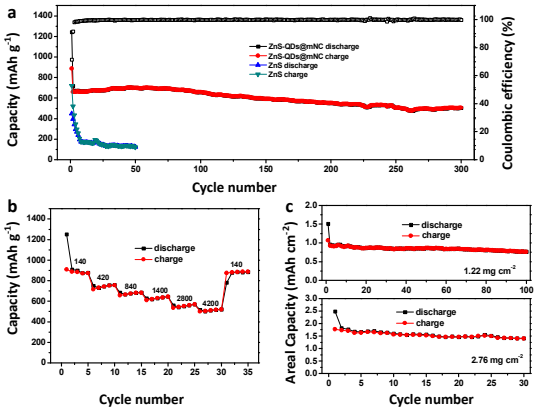

Figure 3. a) Cycling performance of ZnS-QDs@mNC and commercial ZnS with the active material mass loading of 0.70 mg cm^{-2}. Rate was set at 140 mA g^{-1} for the first cycle and 840 mA g^{-1} for later cycles; b) Rate capabilities of ZnS-QDs@mNC at various current densities between 140 and 4200 mA g^{-1}; c) Cycling performances of different mass loading of ZnS-QDs@mNC. All eletrodes were run at 0.3 mA cm^{-2}.

Table 1. Comparison of mass areal loading, areal current density and reversible areal capacity of ZnS/C composites.

Sample	Mass areal loading (mg cm^{-2})	Areal current density (mA cm^{-2})	Reversible areal capacity (mAh cm^{-2})	Ref
ZnS-QDs@mNC	2.76	0.30	1.82	Our work
ZnS@NC	~0.70	0.07	0.49	27
ZnS/NPC	1.04	0.10	0.87	28
ZnS NR@HCP	0.70-0.84	~0.46	~0.44	29
Nano-ZnS-C	0.80	0.08	0.55	30

importance for the practical use. Figure 3c reveals that even when the mass loading of ZnS-QDs@mNC is increased to 2.76 mg cm^{-2}, the stable cycling with a high reversible areal capacity of 1.82 mAh cm^{-2} can still be obtained. Such high areal mass and capacity are outstanding among all recent works on ZnS anode materials (Table 1). To provide further insights, we tested an electrochemical impedance spectrum of ZnS-QDs@mNC before and after 20 cycles (Figure S6). The compressed semicircles at high-medium frequencies describe the charge transfer resistance (R_{ct}) and the inclined lines at low frequency are considered as Warburg impedance (Z_w).[31] The low charge transfer resistance of pristine ZnS-QDs@mNC anode can be attributed to superior conductivity and compact connection between ZnS-QDs@mNC particles. After 20 cycles, the diameter of the semicircle for the ZnS-QDs@mNC electrode becomes much smaller, indicating enhanced kinetics for Li ion insertion/extraction.

To further verify the structure stability of ZnS-QDs@mNC electrode, we examine the volume changes of ZnS-QDs@mNC and ZnS before and after full lithiation by using SEM, as shown in Figure 4. After being fully lithiated, the volume expansion of ZnS reached 70.6%. which was far more than the practical demand (about 30%). As a contrast, the volume expansion of ZnS-QDs@mNC is only 6.5%, which iscomparable to that of commercial graphite.

In order to uncover the reasons behind the structure stability of ZnS-QDs@mNC, we carried out the *in-situ* TEM test to directly observe changes of ZnS-QDs@mNC during lithiation process. As shown in Figure 5a, a potential of -3 V versus Li/Li^+ was applied to drive lithiation when ZnS-QDs@mNC contacts with Li/Li_2O. Noobvious volume expansion and structure demolition of ZnS-QDs@mNC due to lithiation was observed in Movie S1 (supporting Information). The snapshots of ZnS-QDs@mNC before and after lithiation are shown in Figure 5b and 5c. The selected area electron diffraction (SAED) patterns shows that crystalline ZnS quantum dots (inset in Figure 5b) in ZnS-QDs@mNC were transferred into poorly crystalline Li_2S (inset in Figure 5c) after lithiation. Figure 5b shows thelength and width of pristine ZnS-QDs@mNC are 123.5 nm and 147.3 nm, respectively. After lithiation, the length of ZnS-QDs@mNC expands to 135.5 nm due to lithium ions insertion, as illustrated in Figure 5c. However, instead of expansion, the width of ZnS-QDs@mNC contracts to 142.8 nm. The magnified TEM images of the front side of ZnS-QDs@mNC before and after lithiation (Figure 5d and 5e), clearly show that after lithiation the relative positions between carbon nanosheets have changed, which

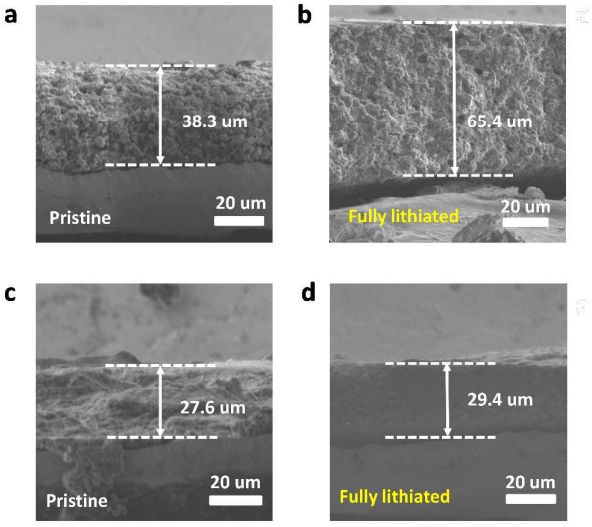

Figure 4. Characterization of volume expansion. Cross-sectional SEM images of ZnS and ZnS-QDs@mNC electrodes (pristine electrodes: a) ZnS and c) ZnS-QDs@mNC; fully lithiated: b) ZnS and nanosheets. d) ZnS-QDs@mNC).

demonstrates that carbon nanosheets slide against each other during lithiation. The similar phenomena are also observed in Figure 5f-i. Such slippage may derive from week interaction between carbon nanosheets and reduction of the interfacial sliding strength causedby the increasing lithium content of the interface of carbon nanosheets.[32] The slippage behavior can help make full use of the limited gaps between carbon nanosheets, thus, resulting in the low volume change of ZnS-QDs@mNC anode (Figure 4d) and the contraction of the ZnS-QDs@mNC width (Figure 5c). Then how about the volume expansions of the ZnS-QDs during lithiation? Would the low volume change of ZnS-QDs@mNC anode be caused by the low volume expansions of ZnS-QDs? To answer the above questions, six ZnS-QDs were selected as samples and measured their size changes before and after lithiation (Figure S7). Obviously, after lithiation, these black quantum dots became grey, which should be caused by Li^+ insertion.[33] Besides, these ZnS-QDs expands isotropically. The corresponding metrical data are summarized in Table S1. The average size expansion of ZnS-QDs is ~27.2%, corresponding to volume expansion of ~105.8% (considering isotropic expansion), which is close to the theoretical value of 110%. Even ZnS-QDs have such large volume expansions and ZnS-QDs@mNC has a high tap density of 0.86 g cm^{-3} and a low total pore volume of 0.092 cm^3 g^{-1}, the volume expansion of the ZnS-QDs@mNC anode is still only 6.5%, which further demonstrates the effectiveness of the slippage behavior in making full use of the limited gaps to accommodate large volume changes of ZnS-QDs. The low volume changes of ZnS-QDs@mNC anode can prevent active materials collapse and separation from the current collector on cycling, thus leading to long-term cycling stability.[34] To explain the isotropic expansion behavior of ZnS-QDs observed in Figure S7, two ZnS quantum dots were chosed as samples, their sizes and corresponding crystal core sizes were measured respectively (Figure S8). And it is observed that the sizes of crystalline cores of ZnS quantum dots are smaller than the dots, which demonstrates that ZnS quantum dots have crystalline/amorphous core-shell structures. Based on theoretical calculations, ZnS nanoparticles with a size in the range 3.9 to 14.2 nm would have crystalline/amorphous core-shell structures.[35] It could be same for ZnS quantum dots with a size around 5 nm. For an amorphous material in which insertion of lithium ions is isotropic,[36] shells of ZnS-QDs would expand isotropically during lithiation. Although insertion of lithium ions is anisotropic for crystalline materials, the sizes of ZnS-QDs crystal cores are so small that the differences between active energies for Li^+ insertion along different directions would be unobvious, resulting in isotropic expansion instead of anisotropic expansion as in a bulk crystal. Therefore, ZnS-QDs (around 5 nm) with crystalline/amorphous core-shell structures would expand isotropically, consistent with the phenomenon we observed in Figure S7. With isotropic expansions of ZnS-QDs,stresses caused by volume changes are absorbed significantly, which can help prevent ZnS-QDs pulverization and separation from the conductive matrix.[36] It is further observed that the lattice fringes of ZnS-QDs disappear afterlithiation (Figure S9), which demonstrates that ZnS-QDs are possibly lithiated to form

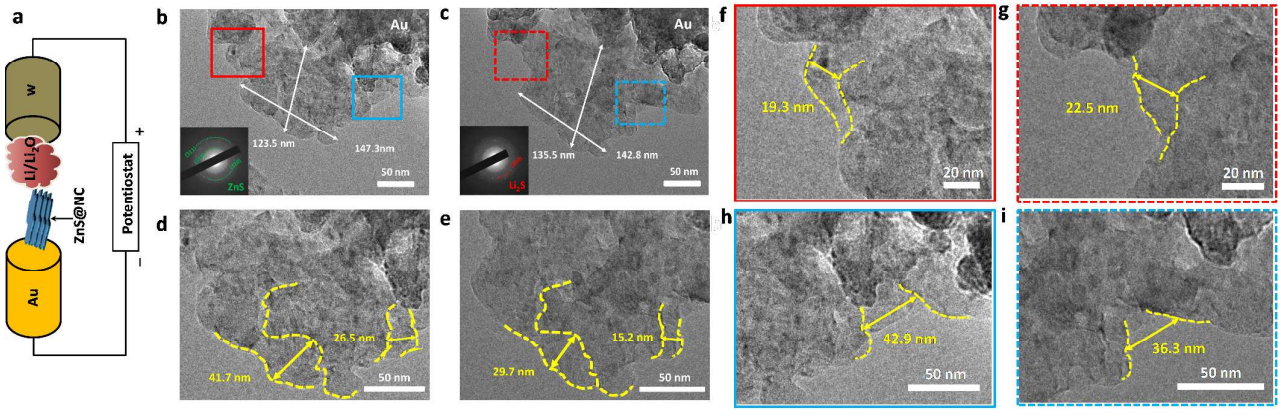

Figure 5. a) Schematic illustration of the in-situ TEM experiment setup. TEM images and SAED patterns of b) pristine and c) fully lithiated ZnS-QDs@mNC. d) and e) Magnified TEM images of the front side of b) and c).f and h) Magnified TEM images of red and blue region outlined in b). g and i) Magnified TEM images of red and blue dotted-line region outlined in c).

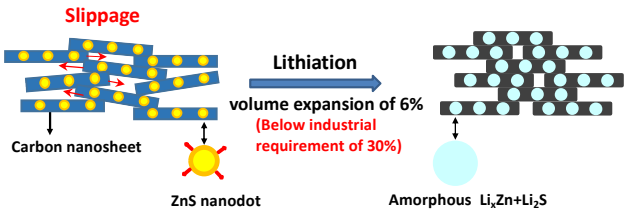

Figure 6. Schematic illustration of ZnS-QDs@mNC before and after lithiation.

amorphous Li_xZn and Li_2S phases, which agrees with the SAED results in Figure 5b and 5c.

As illustrated in Figure 6, the long-term high rate cycling stability of ZnS-QDs@mNC can be attributed the following two main structural advantages. (1) The isotropical expansions of ZnS-QDs can effectively absorb volume-change stresses, avoiding ZnS-QDs pulverization and separation from the carbon frameworks. (2) The slippage of carbon nanosheets can contribute to effectively accommodate large volume changes of ZnS-QDs by making full use of the gaps between carbon nanosheets, leading to the low volume expansion of ZnS-QDs@mNC anode. It should be noted that although we only observe the slippage behaviour during the first lithiation , the slippage behaviour should still works to accommodate volume changes during the following repeated lithiation/dislithiation processes. Otherwise, ZnS-QDs@mNC cannot possess such outstanding cycling stability. The details about the functions of the slippage behaviour in the following repeated lithiation/dislithiation processes need further research.

Conclusions

In summary, inspired by a geological plate-movement in nature, we successfully synthesized ZnS-QDs@mNC with a hierarchically ordered structure, which can effectively accommodate volume changes through the slippage behavior. The slippage behavior is verified by the *in-situ* TEM, which also contributes to a low volume expansion (6.5%) of ZnS-QDs@mNC even with a high tap density of 0.86 g cm^{-3} and a low total pore volume of 0.092 cm^3 g^{-1}. As a result, this materialexhibits outstanding cycling stability (77% capacity retention after 300 cycles) and superior rate performance (over 500 mAh g^{-1} at a high current density of 4200 mA/g). Even at a high mass loading of 2.76 mg cm^{-2} (1.82 mAh cm^{-2}), cycling stability can still be achieved. The novel structure design can be applied to other high-capacity materials to fabricate high-energy-density LIBs anodes.

Experimental

Synthesis of ZIF-7 nanocrystals

All chemicals and solvents were of analytical grade and directly used without purification. 2.72 g $Zn(NO_3)_2 \cdot 6H_2O$ (10 mmol) was dissolved in 100 ml DMF and 2.40 g bIm (20 mmol) was dissolved in 100 ml methanol. After complete dissolution, the two above solutions were mixed at room temperature under magnetic stirring for 30 min. The obtained mixture solution were poured into a glass vessel and then sealed, and the reaction was carried out at 110 ℃ for 2 h. The white precipitation was separated by centrifugation , washed with methanol three times and finally vacuum dried at 100 ℃ over night.

Synthesis of ZnS-QDs@mNC composites

200 mg as-prepared ZIF-7 and 50 mg sulfur powders were completely mixed by grounding together. The mixture was put into a glass tube, evacuated to 8.6x10-6 mbar by a vacuum pump and then sealed quickly. Then the tube was heated from room temperature to 600 ℃ for 1h at a heating rate of 5 ℃ /min in a muffle furnace. After the furnace was cooled to room temperature, the product was taken out; its color changed from white to black. Then the product was washed with a CS2 solution and collected by centrifugation three times(in order to exclude the remaining sulfur). After elimination of sulfur, the products were ball milled for 2h and then dried at 80 ℃ for 12 h.

Materials Characterization

The phase purity and crystal structure of the products were determined by X-ray diffraction (XRD) using a Bruker D8 Focus X-ray diffractometer equipped with a Ni-filtered Cu Kα radiation (λ =0.15406 nm) source. The Raman spectra were recorded using an 514nm Ar-ion laser (LabRAM HR800, Horiba Jobin-Yvon). The morphology and structure of the products were characterized by a scanning electron microscope (SEM, JEOL JSM-7001F) and a transmission electron microscope (TEM, JEOL JEM-2100F). Elemental mapping was performed using a energy dispersive X-ray spectrometry (EDS) attached to the JEM-2100. The BET-specific surface areas of products were calculated from the results of N2 physisorption at 77 K on a Quadrasorb SIMP analyzer. Thermo gravimetric (TG) analysis was performed using a STA7200RV apparatus (HitachiHigh-Tech). Tap density was measured by density analyzer (GeoPyc 1360, micromeritics).

Electrochemical Characterization

The electrochemical measurements were performed at room temperature using CR2025 coin-type half cells. The active material (ZnS-QDs@mNC and commercial ZnS), Super-P carbon black and polyvinylidene fluoride (PVDF) were mixed at a weight ratio of 8:1:1 in N-methyl-2-pyrrolidinone (NMP) solution to form a slurry. The working electrodes were made by pasting the resulting slurry onto copper foils and dried in vacuum at 80 ° C for 12 h. The coin-type cells were assembled in a high pure Ar-filled glove box, using lithium metal as the counter/reference electrode, Celgard 2400 membrane as the separate, and 1M LiPF6 in a mixture of ethylene carbonate (EC), dimethyl carbonate (DMC) and Diethyl carbonate (DEC) (1: 1:1 in volume) as the electrolyte. The cells were galvanostatically charged and discharged on a Neware battery tester in a potential range of 0.01 – 3 V. Electrochemical impedance spectroscopy (EIS) and cyclic voltammetry (CV) measurements were carried out using an Autolab instrument (PGSTAT302N).

Construction of the nano-particle battery

In situ transmission electron microscopy (TEM) observations were conducted in a JEOL-2100F equipped with a “ Nanofactory Instruments AB ” scanning tunneling

microscopy (STM)-TEM holder. In order to build up a test cell, individual ZnS-QDS@mNC particles were attached to the gold wire, which was further attached to the piezo-manipulator. A small piece of lithium foil was also attached to another wolfram wire as a reference and counter electrode. Before insertion of the holder into the TEM, a piece of lithium foil naturally covered with a Li_xO layer was placed on the surface of metal wolfram tip. The lithiation was carried out at a negative bias in the range of -3 V to 0 V with respect to the Li metal.

Conflicts of interest

There are no conflicts to declare.

Acknowledgements

This work was supported by National Key Projects for Fundamental Research and Development of China (No. 2016YFB0100104), National Natural Science Foundation of China (No. 91534109), the "Strategic Priority Research Program" of the Chinese Academy of Sciences (No. XDA09010103), Key program of National Natural Science Foundation of China (No. 91434203) and International Partnership Program for Creative Research Teams (20140491518). X. W. appreciates the support from the "1000 Youth Talent plan" project and the "Excellent One Hundred" project of Beijing JiaoTong University. D.G. is grateful to the Australian Research Council Laureate Project No. FL 160100089.

Notes and references

1 D. C. Lin, Z. D. Lu, P. C. Hsu, H. R. Lee, N. Liu, J. Zhao, H. T. Wang, C. Liu and Y. Cui, *Energy Environ. Sci.*, 2015, **8**, 2371-2376.

2 M. Ko, S. Chae, J. Y. Ma, N. Kim, H. W. Lee, Y. Cui and J. Cho, *Nature Energy*, 2016, **1**, 16113.

3 C. Kim, G. Hwang, J. W. Jung, S. H. Cho, J. Y. Cheong, S. Shin, S. Park and Il-D. Kim, *Adv. Funct. Mater.*, 2017, **27**, 1605975.

4 J. Yu, S.M. Chen, W. J. Hao and S. J. Zhang, *ACS Nano*, 2016, **10**, 2500-2508.

5 H. Wu and Y. Cui, *Nano Today*, 2012, **7**, 414-429.

6 J. J. Zhang and A. Yu, *Sci. Bull.*, 2015, **60**, 823–838.

7 X. D. Xu, W. Liu, Y. Kim and J. Cho, *Nano Today*, 2017, **9**, 604-630

8 W. W. Li, S. M. Chen, J. Yu, D. L. Fang, B. Z. Ren and S. J. Zhang, *Green Energy Environ.*, 2016, **1**, 91-99.

9 Z. L. Xu, X. M. Liu, Y. S. Luo, L. Zhou and J. K. Kim, *Science*, 2017, **90**, 1-44.

10 Y. Zhao, L. P. Wang, M. T. Sougrati, Z. X. Feng, Y. Leconte, A. Fisher, M. Srinivasan and Z. C. Xu, *Adv. Energy Mater.*,2017, 1601424.

11 Y. Zhang, Q. Zhou, J. X. Zhu, Q. Y. Yan, S. X. Dou and W. P. Sun, *Adv. Funct. Mater.*, 2017, **27**, 1702317.

12 N. Liu, Z. D. Lu, J. Zhao, M. T. McDowell, H. W. Lee, W. T. Zhao and Y. Cui, *Nat. Nanotechnol.*, 2014, **9**, 187.

13 C. Wu, J. Maier and Y. Yu, *Adv. Mater.*, 2016, **28**, 174-180.

14 Q. Xu, J. Y. Li, J. K. Sun, Y. X. Yin, L. J. Wan and Y. G. Guo, *Adv. Energy Mater.*, 2016, 1601481.

15 F. Luo, B. Liu, J. Y. Zheng, G. Chu, K. F. Zhong, H. Li, X. J. Huang and L. Q. Chen, *J. Electrochem. Soc.*, 2015, **162**, 2509-2528.

16 X. F. Du, H. L. Zhao, Y. Lu, Z. J. Zhang, A. Kulka and K. Swierczek, *Electrochim. Acta*, 2017, **228**, 100-106.

17 Y. Du,B. Wooler, M. Nines, P. Kortunov, C. S. Paur, J. Zengel, S. C. Weston and P. I. Ravikovitch, *J. Am. Chem. Soc.*, 2015, **137**, 13603-13611.

18 P. L. Lou, Y. B. Tan, P. Lu, Z. H. Cui and X. X. Guo, *J. Mater. Chem. A*, 2016, **4**, 16849-16855.

19 C. X. Li, D. Y. Jiang, L. L. Zhang, J. F. Xia and Q. Li, *Langmuir*, 2012, **28**, 9729-9734.

20 Q. F. Wang , R. Q. Zou , W. Xia , J. Ma , B. Qiu , A. Mahmood , R. Zhao ,Y. Y. C. Yang, D. G. Xia and Q. Xu, *small*, 2015, **11**, 2511-2517.

21 Z. Q. Xie, Z. Y. He, X. H. Feng, W. W. Xu, X. D. Cui, J. H. Zhang, C. Yan, M. A. Carreon, Z. Liu and Y. Wang, *ACS Appl. Mater. Interfaces*, 2016, **8**, 10324-10333.

22 L. Guo, S. Chen and L. Chen, *Colloid Polym. Sci.*, 2007, **285**, 1593-1600.

23 Y. Fu, Z. A. Zhang, X. Yang, Y. Q. Gan and W. Chen, *RSC Adv.,* 2015, **5**, 86941-86944.

24 M. L. Mao, L. Jiang, L. C. Wu, M. Zhang and T. H. Wang, *J. Mater. Chem. A*, 2015, **3**, 13384.

25 Y. Feng, Y. L. Zhang, Y. Z. Wei, X. Y. Song, Y. B. Fub, V. S. Battaglia, *Phys. Chem. Chem. Phys.*, 2016, **18**, 30630.

26 J. Yu, X. Wang, S. M. Chen, X. Y. Liu and S. J. Zhang, *Nano Res.*, 2017, **10**, 172-186.

27 J. M. Li, Y. Fu, X. D. Shi, Z. M. Xu and Z. A. Zhang**,** *Chem. Eur. J.* , 2017, **23**, 157-166.

28 J. B. Li, D. Yan, X. J. Zhang, S. J. Hou, T. Liu, Y. F. Yao and L. K. Pan, *J. Mater. Chem. A*, 2017, **5**, 20428-20438.

29 Z. L. Chen, R. B. Wu, H. Wang, Y. K. Jiang, L. Jin, Y. H. Guo, Y. Song, F. Fang and D. L. Sun, *Chem. Eng. J.*, 2017, **326**, 680-690.

30 X. F.Du, H. L. Zhao, Z. J. Zhang, Y. Lu, C. H. Gao, Z. L. Li, Y. Q. Teng, L. N. Zhao and K. Swierczek, *Electrochim. Acta.*, 2017, **225**, 129-136.

31 K. N. Zhao, L. Zhang, R. Xia, Y. F. Dong, W. W. Xu, C. J. Niu, L. He, M. Y. Yan, L. B. Qu and L. Q. Mai, *small*, 2016, **12**, 588-594.

32 M. Stournara, X. C. Xiao, Y. Qi, P. Johari, P. Lu, B. Sheldon, H. J. Gao and V. Shenoy, *Nano Lett.*, 2013,**13**, 4759-4768.

33 Q. M. Su, S. X. Wang, Y. L. Xiao, L. B. Yao, G. H. Du, H. Q. Ye and Y. Z. Fang, *J. Phys. Chem. C*, 2017, **121**, 3295-3303.

34 S. J. Hao, B. W. Zhang, J. Y. Feng, Y. Y. Liu, S. Ball, J. S. Pan, M. Srinivasan and Y. Z. Huang, *J. Mater. Chem. A*, 2017, **5**, 8510-8518

35 A. S. Barnard, C. A. Feigl and S. P. Russo, *Nanoscale*, 2010, **2**, 2294-2301.

36 Z. M. Tu, G. Z. Yang, H. W. Song and C. X. Wang, *ACS Appl. Mater. Interfaces*, 2017, **9**, 439-446.

Inspired by geological plate movements in releasing the inner stresses of the earth, a ZnS anode material, composed of ZnS quantum dots@carbon nanosheets stacked together, is designed for high-energy Li-ion Batteries.